

# Interpolation and Denoising of Seismic Data using Convolutional Neural Networks

Sara Mandelli, Vincenzo Lipari, Paolo Bestagini, *Member, IEEE*, and Stefano Tubaro, *Senior Member, IEEE*

**Abstract**—Seismic data processing algorithms greatly benefit, or even require regularly sampled and reliable data. Therefore, interpolation and denoising play a fundamental role as starting steps of most seismic data processing pipelines.

In this paper, we exploit convolutional neural networks for the joint tasks of interpolation and random noise attenuation of 2D common shot gathers. Inspired by the great contributions achieved in image processing and computer vision, we investigate a particular architecture of convolutional neural network known as *U-net*, which implements a convolutional autoencoder able to describe the complex features of clean and regularly sampled data for reconstructing the corrupted ones. In training phase we exploit part of the data for tailoring the network to the specific tasks of interpolation, denoising and joint denoising/interpolation, while during the system deployment we are able to retrieve the remaining corrupted shot gathers in a computationally efficient procedure.

In our experimental campaign, we consider a plurality of data corruptions, including different noise models and missing traces' distributions. We illustrate the advantages of the aforementioned strategy through several examples on synthetic and field data. Moreover, we compare the proposed denoising and interpolation technique to a recent state-of-the-art method.

**Index Terms**—Interpolation, Noise attenuation, Seismic data, Convolutional Neural Network.

## I. INTRODUCTION

SEISMIC data surveying is one of the main methods for gaining information about the physical properties of the Earth's subsurface. One of the main goals of processing the resulting data is the management of natural resources such as energy sources and fresh water. In this context, seismic processing methods are essential to discover, localize and characterize economically worthwhile geological reservoirs, such as hydrocarbons accumulations, and to manage the extraction of the resources stored in them.

The quality of the acquired data, both in term of Signal-to-Noise Ratio (SNR) and of regularity and density of its sampling, is crucial to achieve a reliable interpretation of the subsoil. Unfortunately, such data is inevitably heavily corrupted by both random and coherent noise. An additional problem is that economic limitations, cable feathering, environmental constraints and elimination of badly acquired traces cause irregular spatial sampling in almost all seismic acquisitions.

S. Mandelli, V. Lipari, P. Bestagini and S. Tubaro are with the Dipartimento di Elettronica, Informazione e Bioingegneria, Politecnico di Milano, Milano 20133, Italy (e-mail: name.surname@polimi.it).

The authors would like to thank Lingchen Zhu for having released the detailed implementation of the double-sparsity dictionary learning method, including a clarifying explanation and useful suggestions.

Unfortunately, most state-of-the-art seismic processing algorithms, such as reverse-time-migration [1], full-waveform-inversion [2] and surface related multiple elimination [3] require high quality regularly sampled data. Consequently, a vast majority of seismic processing pipelines require data pre-processing steps, including effective denoising and trace interpolation algorithms. Moreover, due to the increasing size of the acquired data, a key factor of these procedures for industrial application is their computational burden, in terms of both memory requirements and computational time.

The problems of trace interpolation and noise attenuation have been widely investigated, either simultaneously or separately. Among the dozens of interpolation methods have been proposed so far, we can roughly identify four main categories.

Model-based algorithms implement an implicit migration-demigration pair [4], [5]. A major drawback of these techniques is that their performance is strongly affected in case of complex structural burden.

A second approach is based on prediction filters [6], which assume seismic data to be a (local) superposition of plane waves. However, these methods target regularly sampled data, which is a heavy limitation.

Due to their repetitive features, clean seismic data are intrinsically low-rank in the time-space domain. Conversely, noise and missing traces increase the rank of the data [7]. Therefore, algorithms recasting the interpolation (and denoising) problems as rank reduction and matrix/tensor completion have been largely studied in the past decade as third alternative to the problem [8]–[12].

A great amount of denoising and interpolation algorithms exploit a transform domain where the clean signal can be represented only by few non-zero coefficients and therefore clean data and noise are more easily separable. The rationale behind this forth family of methods is that noise and missing traces map in non-sparse artifacts in the transform domain.

Several fixed-basis sparsity-promoting transforms have been widely used also for seismic data interpolation. Among the various approaches, coming from different fields, we can cite: the Fourier transform [13], the Hilbert-Huang transform [14], [15], the time-frequency peak filtering, [16]–[18], the Radon transform [19], different curvelet-like transforms [20]–[25] and the EMD-seislet transform [26]. These transform methods implicitly assume regularity of the data described by analytic models, resulting in fixed dictionaries. However, these dictionaries can be thought as defining only a subset of the transforms methods.

Alternatively, data driven sparse dictionaries can be learned directly from the dataset. In other words, these methods

assume that clean signals are a linear combination of the atoms in a learned overcomplete dictionary. Learned dictionaries, in the form of explicit matrices for small patches, usually better match the complex data characteristics. For instance, denoising results obtained using double sparse dictionary learning and outperforming fixed dictionary transforms have been reported in [27] and [28], combining the dictionary learning based sparse transform with the fixed-basis transform, which is called double-sparsity dictionary. Recently, Zhu et al. [29] introduced a joint seismic data denoising and interpolation using a masking strategy in the sparse representation of the dictionary.

In the latest years, the outstanding advancements brought by deep learning and Convolutional Neural Networks (CNNs) have greatly impacted the whole signal and image processing community. In this context, innovative strategies for data interpolation and denoising based on deep learning have been proposed in manifold image processing tasks. Indeed, solutions based on CNNs are nowadays often exceeding state-of-the-art results. However, these methods have barely started to be explored by the geophysical community for the problems of denoising and interpolation. Promising results for the aforementioned tasks have been reported through residual neural networks [30], [31], generative adversarial networks [32] and convolutional autoencoders [33], [34].

In this paper we elaborate on the method we proposed for simple interpolation [33], extending it to both interpolate and denoise irregular 2D seismic data directly in the shot-gather domain. Inspired by the important contributions achieved in image processing problems, we propose to exploit a properly trained *U-net* [35] as a strongly competitive strategy for noise attenuation and reconstruction of missing traces in pre-stack seismic gathers. We provide examples on synthetic and field data showing promising performances on either denoising, interpolation, or joint denoising and interpolation problems. The results obtained for the joint interpolation and denoising task also outperform a recent state-of-the-art technique taken as reference.

The rest of the paper is organized as follows. In Section II, we introduce the proposed network architecture, justifying the use of CNNs for interpolation and denoising of 2D seismic data. In Section III, we present the specific pipeline to be followed in order to train and test the *U-net* for reconstructing corrupted gathers. In Section IV, the proposed method is applied to synthetic and field 2D seismic data. Each building block is separately validated, and the joint interpolation and denoising strategy is also compared to a state-of-the-art method. Eventually, in Section V, we discuss the advantages and the potential issues of our method and draw conclusions.

## II. PROBLEM STATEMENT AND BACKGROUND ON AUTOENCODERS

In this section, we first report details about the formulation of the tackled problems, namely interpolation and/or denoising of seismic data. Then, we provide some background concepts on Convolutional Autoencoders (CAs) and how to exploit them for our specific goals, which is useful to understand the rest of the paper.

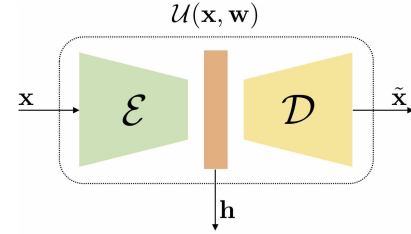


Fig. 1: Scheme of a Convolutional Autoencoder architecture.

### A. Problem formulation

In this paper, we focus on the problem of reconstructing seismic gathers which have been corrupted by irregular trace sampling and/or additional noise. Formally, we represent each original non-corrupted seismic gather as  $\mathbf{I}$ , whether its corrupted version is denoted as  $\tilde{\mathbf{I}}$ . Our goal is estimating a clean and dense version of the seismic data, namely  $\hat{\mathbf{I}}$ , as similar as possible to the original corresponding gather  $\mathbf{I}$ .

In order to solve this problem, we make use of a particular kind of convolutional neural network named Convolutional Autoencoder (CA). Our choice is motivated by the great capability of CA in learning compact representations of the data, and by the strong computational efficiency in reconstructing the corrupted ones. In the following, we report some backgrounds on CAs, introducing the specific network architecture exploited for the prescribed task.

### B. Convolutional Autoencoders for interpolation and denoising

Convolutional Autoencoders (CAs) are convolutional neural networks whose architecture can be logically split in two separate components: the encoder and the decoder. Precisely, the CA structure is sketched in Fig. 1: (i) the encoder, represented by the operator  $\mathcal{E}$ , maps the input  $\mathbf{x}$  into the hidden compact representation  $\mathbf{h} = \mathcal{E}(\mathbf{x})$ ; (ii) the decoder, represented by the operator  $\mathcal{D}$ , transforms the hidden representation into an estimate of the input  $\tilde{\mathbf{x}} = \mathcal{D}(\mathbf{h})$ .

For image processing problems, CA proves to be a very powerful instrument for inpainting and denoising tasks [36], [37]. The rationale behind the use of CA for inpainting and denoising shares some common concepts with the transform-based and dictionary learning techniques.

Indeed, CA is trained so that the encoder part results in a compact representation of clean data, where the interference due to noise and missing samples is not mapped. Therefore, if the compact representation is correctly built, the result of the decoder is a *dense* clean image without missing samples. Consequently, it is possible to train a CA to learn a hidden representation of the clean data in common shot gathers and then to recover clean and densely sampled gathers from noisy and scattered ones.

In particular, in this work we exploit a CNN architecture known as *U-net*. Originally designed for image segmentation problems and then used for several different tasks [38], the *U-net* is named after the shape it is usually graphically represented with. Indeed, *U-net* shares a large part of the

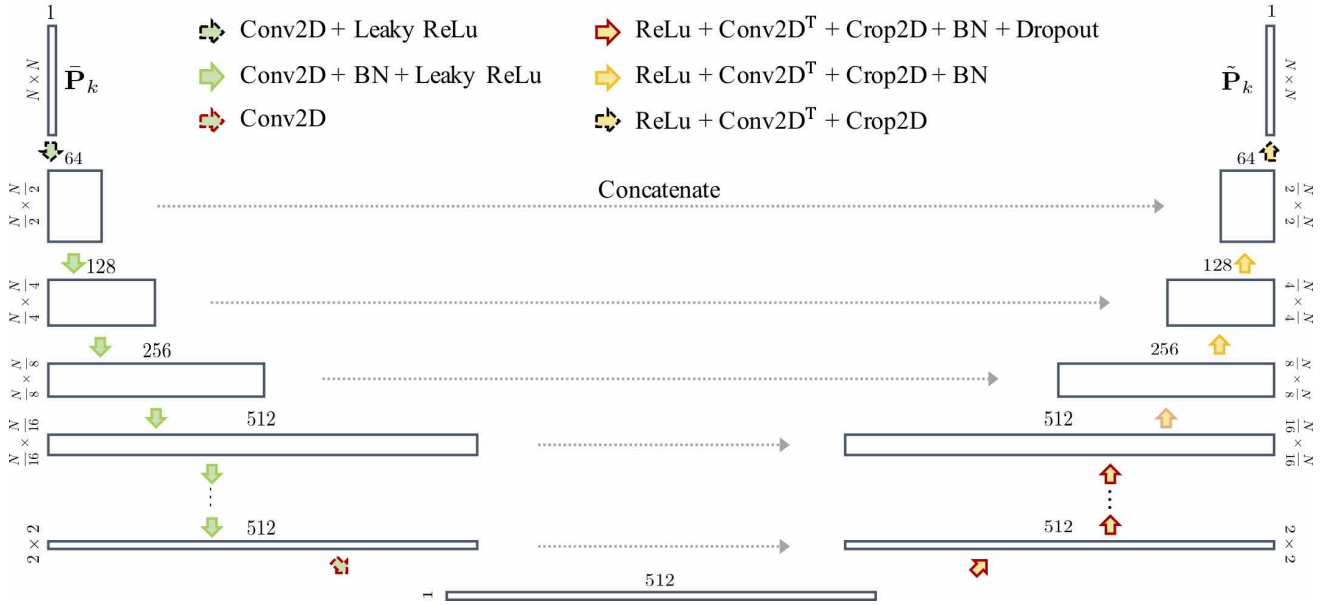


Fig. 2: Architecture of the used *U-net*.

architecture with classical CA. However, in a *U-net*, the representations of the input obtained at different levels of the encoder are directly concatenated to the corresponding decoder levels. For the sake of brevity, we refer the interested readers to [35] for a detailed explanation of these architectures.

Continuing the analogy with the transform-based methods, we can think the trained *U-net* as an instrument implicitly providing a multi-scale/multi-resolution hidden representation, able to describe the complex features of clean seismic data where noise and missing data are not modeled. By using a computer vision terminology, we can think at the interpolation and denoising task as an image transfer problem, with the goal of transforming gathers corrupted by noise and/or missing traces into regularly sampled clean gathers.

### III. RECONSTRUCTING THE CORRUPTED GATHERS

In this section we explain how to reconstruct the corrupted seismic gathers. In particular, we report all the technical details concerning the used network architecture, then we describe two solutions for the network training, to be used according to the specific data corruption. Eventually we describe the system deployment, that is, whether a corrupted gather is under investigation, how to correctly reconstruct it as similar as possible to the original one.

#### A. Implementation of *U-net*

Following the same rationale behind our previous investigations [33], we propose to work in a patch-wise fashion, as this allows to focus on local portions of the image and to ensure a sufficiently large amount of data under analysis. Specifically, we divide each gather into  $K$  patches of size  $N \times N$ .

Despite this similarity with [33], in this paper we introduce quite a few novelties with respect to our past studies in order to simplify the network architecture at highest levels and enhancing the system efficiency without drops in performances.

For instance, as seismic data typically has a value range very different from that of natural digital images for which CNNs are typically studied, each patch is scaled by a constant gain  $G$ , which proves to be more effective than our previous data normalization procedure in terms of speed convergence and achieved validation results. Considering that corrupted gathers are labeled as  $\tilde{\mathbf{I}}$ , the generic  $k$ -th corrupted patch given as input to the network is denoted as  $\tilde{\mathbf{P}}_k$ .

As *U-net* like architectures turn out to be the state-of-the-art for the tasks of image inpainting [39], [40] and denoising of medical images [41], we follow the trend started by [35], exploiting a *U-net* architecture composed by the blocks shown in Fig. 2:

- 1) A number of stages where a 2D Convolution with filter size  $4 \times 4$  and stride  $2 \times 2$ , sometimes followed by Batch Normalization (BN) and/or Leaky ReLu, is performed. These stages lead to the hidden representation (i.e., the result of the encoding part). It is worth noting that the number of filters increases from 64 to 512 as we go deep into the network.
- 2) The same number of stages as before where a ReLu, a 2D Convolution with filter size  $4 \times 4$  and stride  $2 \times 2$  and a 2D cropping, possibly followed by BN and Dropout are performed. In each stage we concatenate the result of the corresponding encoding stage as in a typical *U-net* fashion. Note that the number of filters is gradually diminished as we go up in the right path of the network (i.e., decoding path). The last stage outputs the patch  $\hat{\mathbf{P}}_k$ , of the same size of the input patch.

Notice that, with this architecture, there is no need to additionally consider the gradient computation and the batch normalization step after the first convolutional layer as proposed in [33]. This makes the proposed approach leaner. Additionally, the overall architecture scales according to the patch dimension  $N$ , which can be selected depending on possible application-driven constraints. Anyway, as the network can be

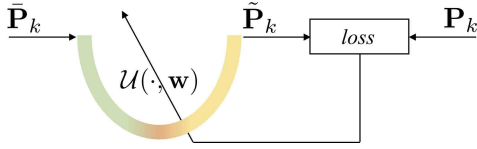


Fig. 3: Training phase.

characterized by more than 40 million parameters, it needs to be trained on a significant amount of seismic images as any typical deep learning solutions.

### B. U-net training

Once defined the network architecture, the key point is the design of the training strategy through a proper definition of the cost function tailored to our specific problem. Indeed, the *U-net* defines a parametric model  $\tilde{\mathbf{x}} = \mathcal{U}(\mathbf{x}, \mathbf{w})$ , between the output  $\tilde{\mathbf{x}}$  and the input  $\mathbf{x}$  and network weights  $\mathbf{w}$ . The training phase consists in estimating the network weights  $\mathbf{w}$  through the minimization of a distance metrics between the network input and its output. This distance is usually referred as *loss* function, and its minimization is carried out using iterative techniques (e.g., stochastic gradient methods, etc.).

Specifically, as shown in Fig. 3, we train the network in order to transform patches  $\bar{\mathbf{P}}_k$ , extracted from gathers corrupted by noise and/or missing traces, into regularly sampled and clean patches  $\tilde{\mathbf{P}}_k$ . As in any supervised learning problem, we assume to have a training dataset  $\mathcal{D}_T$  and a validation dataset  $\mathcal{D}_V$ , each one composed by pairs of corrupted/uncorrupted gathers  $(\bar{\mathbf{I}}, \mathbf{I})$ .

These datasets are exploited for estimating the network parameters  $\mathbf{w}$  and to decide when to stop the cost function minimization process. Actually, the training stage slightly differs depending of the specific problem: denoising only, interpolation only, and joint denoising/interpolation.

For denoising only and joint denoising/interpolation, model weights are estimated by minimizing the *loss* function between  $\mathbf{P}_k$  and  $\tilde{\mathbf{P}}_k$ , defined as the squared error over all patches belonging to gathers in the training set  $\mathcal{D}_T$ . Formally,

$$\mathbf{w} = \arg \min_{\mathbf{w}} \sum_{\mathbf{P}_k \in \mathcal{D}_T} \left\| \mathbf{P}_k - \tilde{\mathbf{P}}_k(\mathbf{w}) \right\|_{\mathbb{F}}^2, \quad (1)$$

where  $\|\cdot\|_{\mathbb{F}}$  represents the Frobenius norm and, with a slight abuse of notation,  $\mathbf{P}_k \in \mathcal{D}_T$  denotes patches extracted from gathers belonging to training dataset.

However, for the task of interpolation only, we a-priori know that only some samples need to be reconstructed by the network (i.e., the missing ones), whereas the others can be left untouched. For this reason, the *loss* is evaluated only on inpainted samples. This is implicitly performed by adding a masking stage that sets to zero all uncorrupted traces. Network weights are then estimated as

$$\mathbf{w} = \arg \min_{\mathbf{w}} \sum_{\mathbf{P}_k \in \mathcal{D}_T} \left\| (\mathbf{P}_k - \tilde{\mathbf{P}}_k(\mathbf{w})) \otimes \mathbf{M} \right\|_{\mathbb{F}}^2, \quad (2)$$

where  $\otimes$  represents the Hadamard product and  $\mathbf{M}$  is a binary mask of size  $N \times N$  defined as

$$[\mathbf{M}]_{i,j} = \begin{cases} 1 & \text{if } [\bar{\mathbf{P}}_k]_{i,j} \text{ is a missing sample} \\ 0 & \text{otherwise.} \end{cases} \quad (3)$$

As in standard neural network training, we follow an iterative procedure to minimize either (1) or (2), stopping at the iteration where the mean squared error over all the patches  $\mathbf{P}_k \in \mathcal{D}_V$  is minimum.

Specifically, we use Adam optimization algorithm [42], with learning rate and patience initialized at 0.01 and 10, respectively. The former is decimated while the latter is halved in presence of plateau of the cost function. In general, we train the network for a maximum number of 100 epochs, although we verified the smallest loss on validation patches is often achieved within the first 30 training epochs.

### C. System Deployment

When a new corrupted gather  $\bar{\mathbf{I}}$  belonging to evaluation set  $\mathcal{D}_E$  is under analysis, its recovered version is estimated following the scheme depicted in Fig. 4.

First of all, a set of  $K$  patches is extracted from image  $\bar{\mathbf{I}}$  as described in Sect. III-B. Then, each patch  $\bar{\mathbf{P}}_k$  is processed by the *U-net* architecture in order to estimate the patch  $\tilde{\mathbf{P}}_k$ .

Following the same logic of the training phase, the estimated patches are post-processed in slightly different ways according to the specific goal. For denoising only and joint denoising/interpolation, each patch  $\tilde{\mathbf{P}}_k$  simply undergoes a denormalization step, thus it is divided by the gain  $G$  to obtain the output patch  $\hat{\mathbf{P}}_k$ . Concerning the task of interpolation only, it is reasonable to leave the known samples untouched in the final estimated patch. Therefore, exploiting the binary mask defined in (3), each patch  $\hat{\mathbf{P}}_k$  is obtained as

$$\hat{\mathbf{P}}_k = \frac{\bar{\mathbf{P}}_k \otimes \bar{\mathbf{M}} + \tilde{\mathbf{P}}_k \otimes \mathbf{M}}{G}, \quad (4)$$

being  $\bar{\mathbf{M}}$  the logical complement of  $\mathbf{M}$ .

Eventually, in order to reconstruct the image gather  $\hat{\mathbf{I}}$ , all the estimated patches  $\hat{\mathbf{P}}_k$  are re-assembled together, sample-wise averaging the overlapping portions if some overlap between patches was used during patch extraction procedure.

## IV. RESULTS

In this section we present the result of our experimental campaign obtained on well-known public datasets. Specifically, we evaluate our methodology over both synthetic and field data. First, we introduce the accuracy metrics we exploit for evaluating the results. Second, we separately validate the performances of the proposed interpolation and denoising strategies on both synthetic and real data. Finally, we investigate the combined interpolation and denoising problem also comparing our method against a state-of-the-art solution.

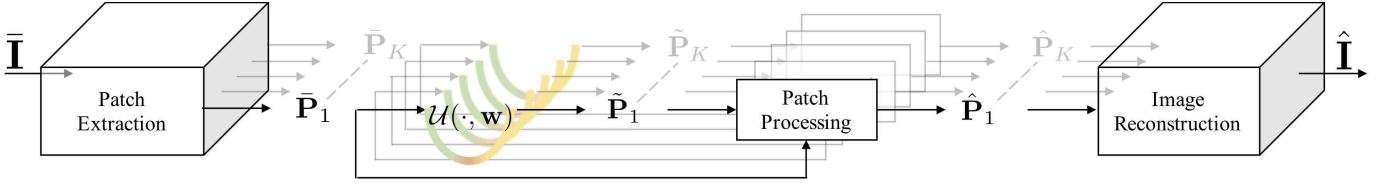


Fig. 4: Proposed pipeline for recovering each corrupted gather  $\tilde{\mathbf{I}}$ .

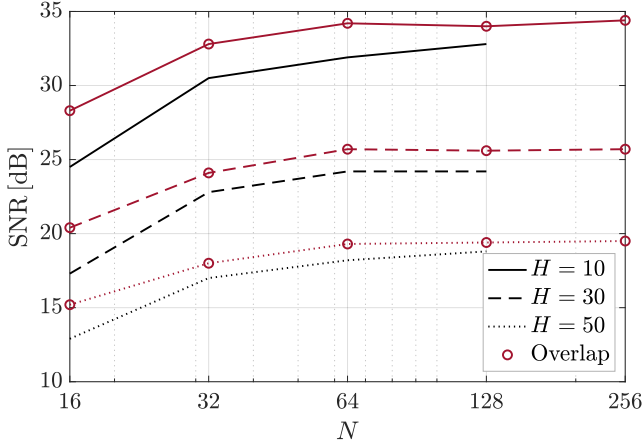


Fig. 5: Average SNR [dB] achieved on gathers belonging to  $\mathcal{D}_E$ , as function of patch dimension  $N$  and overlap.

#### A. Accuracy metrics

We evaluate the performances of our method in reconstructing each entire seismic image belonging to the evaluation set  $\mathcal{D}_E$ , namely the corrupted gathers which have never been seen by the *U-net*. The accuracy metrics is the SNR, defined as the ratio between the variance of the original gather and of the reconstruction error, hence:

$$\text{SNR} = 10 \log_{10} \frac{\sigma^2(\mathbf{I})}{\sigma^2(\mathbf{I} - \hat{\mathbf{I}})} \quad \mathbf{I} \in \mathcal{D}_E, \quad (5)$$

where  $\sigma^2(\cdot)$  computes the variance.

#### B. Problem 1: Interpolation of missing traces

In this section we present the network performances in interpolating gathers with missing traces. In particular, we start showing results achieved over a synthetic dataset, considering various interpolation situations. Finally, we evaluate the proposed strategy on real field data.

1) *Synthetic data*: The reference dataset used to systematically explore the results is extracted from the well known synthetic BP-2004 benchmark [43]. In particular, we work with 1348 shot gathers, cropped at the first 1152 traces (taking the source as reference) and at the first 1920 time samples/trace. The central frequency of each trace is 27Hz, sampled every  $\delta_t = 6\text{ms}$ , and the group spacing is 12.5m.

In order to properly evaluate the proposed method, we randomly split the dataset into training, validation and evaluation, using 250 shot gathers for training and validation (further split on 75% of images for training set  $\mathcal{D}_T$ , and 25% for validation set  $\mathcal{D}_V$ ), and the remaining for evaluation set  $\mathcal{D}_E$ .

#### a) Interpolation of uniformly distributed missing traces:

The first experiment investigates the situation of random missing traces with uniform distribution. This choice follows the main reasoning of the works proposed in literature, as well as our previous contribution regarding shot gather interpolation [29], [33], [44].

In order to simulate the uniform lack of seismic acquisitions, we extract 3 different datasets from the reference one, deleting a percentage  $H$  of the available data traces. To be precise, for each shot gather  $\mathbf{I}$ , we randomly delete the  $H\%$  of its traces,  $H \in \{10, 30, 50\}$ , obtaining a holed gather  $\tilde{\mathbf{I}}$ .

As shown in Section III-A, we work in patch-wise fashion for reconstructing the corrupted gathers. Specifically, each gather entering the network is initially split into a plurality of squared patches, with dimensions  $N \times N$ . In light of this, we perform an initial experiment to analyze the network output behaviour as function of the specific input data. Precisely, the goal of this primary investigation is to select a good patch extraction method, that is, the strategy leading to the highest reconstruction accuracy on the evaluation set. We consider different values for  $N$ , namely  $N \in \{16, 32, 64, 128, 256\}$ , and we evaluate the cases of non-overlapping patches and of patches extracted with an overlap of  $N/2$  in both directions.

To evaluate the *U-net* performances according to the chosen patch extraction method, we use SNR defined in (5). Fig. 5 shows the average SNR achieved over gathers belonging to evaluation set, with and without the overlap between the extracted patches. Note that the case  $N = 256$  does not include results without overlap because the gather dimensions are not integer multiples of this value. It is noticeable that small values of  $N$  are not good solutions for reconstructing the corrupted images, probably because the *U-net* needs to analyze more samples together in order to find a good hidden representation of the input patch. As expected, introducing some overlap during patch extraction always returns better performances than just selecting adjacent patches. This is due to two main factors: first, selecting overlapped patches increases the amount of data seen by the network and reasonably improves its performances; second, in the image reconstruction phase, the overlapping portions of the patches are averaged one another, decreasing the possibility to generate undesired border effects.

Even if selecting an overlap of  $N/2$  gives slightly better results, one consideration must be done. At training stage, we found out that a good strategy is to group in a single batch all the patches extracted from the same shot gather, ending up with a batch size (i.e., the amount of *patches* in a batch) strictly dependent on  $N$ . Notice that the number of *samples* per batch does not change with  $N$ , if patches are



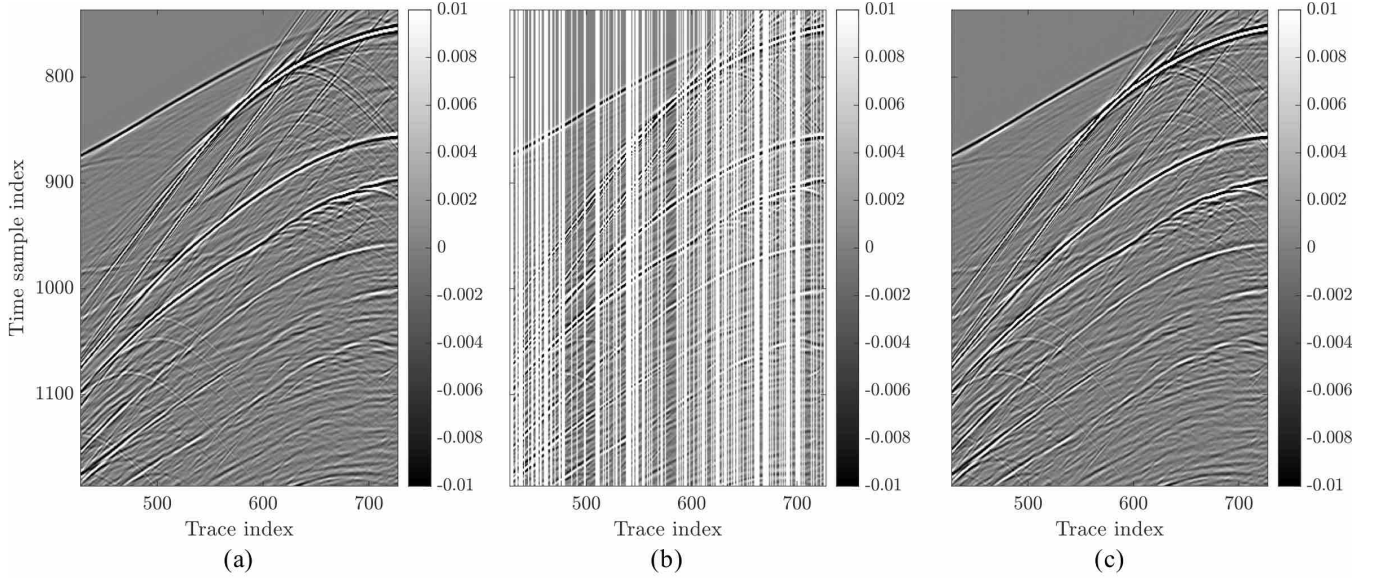


Fig. 6: Example of data interpolation considering one gather of the synthetic dataset. Precisely, (a) depicts the original gather  $\mathbf{I}$ , cropped in its central portion with size  $450 \times 300$ ; (b) reports the corrupted gather  $\bar{\mathbf{I}}$ , with 50% of randomly missing traces, (c) shows the reconstructed gather  $\hat{\mathbf{I}}$ .

not overlapped. Conversely, in case of overlapped patches, the number of samples per batch increases, as some samples belong to multiple patches. Therefore, the higher the overlap, the larger the amount of GPU memory required in training phase. If the absence of overlap requires a GPU memory usage more or less equal to 4GB for every  $N$ , in case of overlap the required space increases in a quadratic fashion.

Therefore, considering that the achieved SNR performances of the two methodologies (overlapped and non-overlapped patches) are not so far one another, we choose the patch extraction strategy which selects only adjacent and non-overlapping patches. For this reason, hereinafter we only investigate the network behavior considering non-overlapped patches, as overlapping would make the solution impractical in the majority of use cases.

Regarding the patch dimension  $N$ , as the SNR curve monotonically increases with the patch dimension but without dropping performances in terms of memory usage, we select  $N = 128$  for all the experimental campaign. We end up with batches of 135 non overlapping patches with dimensions  $128 \times 128$  extracted from each shot gather. Consider that the process involves more than 25 000 training patches, more than 8 500 validation patches, and more than 145 000 testing patches for each dataset.

Regarding the results, we are able to achieve SNR of 32.8dB, 24.2dB and 18.8dB for  $H = 10, 30$  and  $50$ , respectively. The processed gathers do not visually show any artifacts due to the interpolation method, even in the worst case given by  $H = 50$ , as depicted by the example in Fig. 6.

*b) Interpolation of bursts of missing traces:* Uniform distribution of missing traces, described by the percentage  $H$ , allows the evaluation of average reconstruction performances of the interpolation. However, in order to have a more detailed description, here we study the performances of the proposed

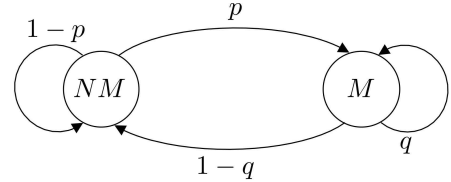


Fig. 7: Markov chain of the burst corruption model.

*U-net*-based interpolation on a more sophisticated corruption model. Basing on the consideration that missing traces (due for instance to spatial obstacles) are likely to appear in groups, we propose a burst missing traces model inspired by the packet loss models of telecommunication networks [45].

In particular, the model is a two states Markov model described by two parameters,  $\alpha$  and  $\beta$ :  $\alpha$  refers to the probability of a missing trace, while  $\beta$  is the average length of the burst, i.e., the average number of missing traces which are adjacent one another.

The Markov chain of the model is depicted in Fig. 7, where  $NM$  represents the non-missing trace state whereas  $M$  is the state for missing trace. The probability to find a corrupted trace, given that the previous one (in the spatial dimension) was missing, is  $q$ , while the probability to pass from a non missing trace to a missing one is  $p$ . These probability values can be derived from  $\alpha$  and  $\beta$ , formally,

$$q = 1 - \frac{1}{\beta}, \quad p = \frac{\alpha}{\beta(1-\alpha)}. \quad (6)$$

Exploiting this model, we can simulate more realistic scenarios, where bursts of adjacent missing traces can occur, due for instance to environmental constraints or sudden interruptions during acquisitions. In order to test our method on this missing trace distribution, we select various percentage of missing traces  $\alpha \in \{10, 30, 50\}\%$  with average burst

TABLE I: Average SNR [dB] achieved on gathers belonging to  $\mathcal{D}_E$ , for different values of  $\alpha$  and  $\beta$ .

$\alpha \backslash \beta$	1	2	3
10	38.4	25.3	21.9
30	32.8	21.7	18.1
50	29.9	18.7	15.7

length  $\beta \in \{1, 2, 3\}$ , corresponding to 12.5m, 25m and 37.5m respectively. Notice that, the larger the average gap, the greater the gap size dispersion. Indeed, for  $\beta = 1$  the standard deviation is equal to  $\sigma = 0$  traces (isolated missing traces only); on the contrary, for  $\beta = 2$  and  $\beta = 3$  the standard deviations are  $\sigma = 1.14$  and  $\sigma = 2.44$  traces, respectively. For instance, in the datasets under examination,  $\beta = 3$  provides a maximum gap up to 30 traces (corresponding to 375m), which simulates a quite large physical obstacle.

Table I depicts the average results achieved by the *U-net* on the evaluation set. Notice that, the larger the burst length, the lower the resulting SNR. This enlightens the need of further investigations for interpolating bursts of many traces: as a matter of fact, as the group of adjacent missing traces increases, the ability of the network in reconstructing the unknown samples diminishes. Nonetheless, notice that even in the worst case, i.e.,  $(\alpha, \beta) = (50, 3)$ , the *U-net* is able to maintain acceptable reconstruction performances.

*c) Interpolation by transfer learning:* In order to test the robustness of the proposed method in interpolating missing data, we generate two further synthetic datasets, exploiting the very same acquisition geometry and model of the dataset presented in IV-B1, but with different sampling rates 4ms and 8ms. The goal of this experiment is to check if the *U-net* architecture, when trained on data sampled every 6ms, is able to reconstruct differently-sampled data. This is an example of the well-known transfer learning strategy. Namely, it corresponds to analyzing the performances of one network which has already been trained over a dataset having different features from the testing one.

To this purpose, we propose to select as test case the uniform missing traces framework, randomly deleting the 30% of traces from these new datasets. Then, we evaluate the reconstruction results on gathers belonging to the evaluation set  $\mathcal{D}_E$  of these datasets, with the difference that we exploit the network trained on the dataset sampled every  $\delta_t = 6$ ms.

Average results of the interpolation are shown in Table II. Notice that we report also the interpolation results we can achieve if following the standard training pipeline, that is, training the network using data with the same sampling time of the evaluation set. Even if the difference between the results is noticeable, Fig. 8 shows an example of  $\delta_t = 8$ ms data reconstruction exploiting the *U-net* trained on  $\delta_t = 6$ ms. It is noticeable that the error is concentrated in the upper part of the gather, while in the higher energy regions the reconstruction is quite good and acceptable.

2) *Field data:* In this section, we propose to apply the *U-net* for reconstructing corrupted real seismic data. To this

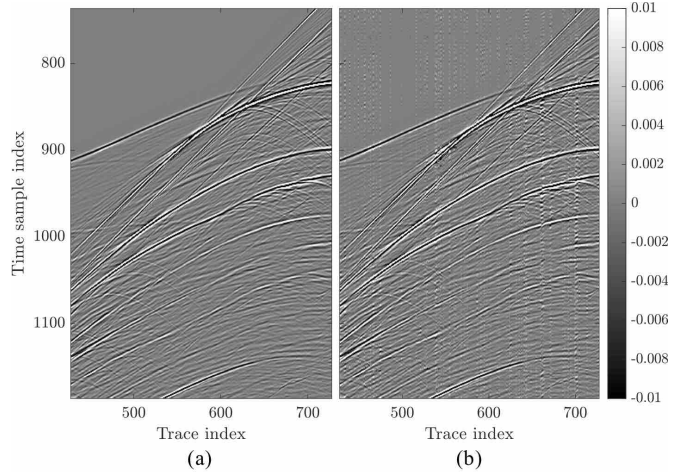


Fig. 8: Example of transfer learning data interpolation. Precisely, (a) depicts the original gather  $\mathbf{I}$ , sampled every 8ms and cropped in its central portion with size  $450 \times 300$ , (b) shows the reconstructed gather  $\hat{\mathbf{I}}$ , exploiting the *U-net* trained on data sampled every 6ms.

TABLE II: Average SNR [dB] achieved on  $\mathcal{D}_E$ , for sampling time  $\delta_t = 4$ ms and  $\delta_t = 8$ ms.

$\delta_t$	4ms	8ms
Train on 6ms	10.1	10
Train on $\delta_t$	25.3	23.8

purpose, we exploit as field data the well known Mobil Avo Viking Graeben Line 12 dataset [46]. The example repeats what already presented in [33] while improving the results thanks to a slightly different network architecture and data pre-processing. Specifically, this dataset consists of 1001 marine shot gathers. Each gather is composed of 128 traces of 1408 time samples, with temporal sampling of 4ms and receiver sampling of 25m.

In order to compare our results with the previously achieved ones, we simulate the uniform lack of seismic acquisition. Therefore, for each acquired gather  $\mathbf{I}$ , we randomly delete the  $H\%$  of its traces,  $H \in \{10, 30, 50\}$ , obtaining a scattered sampled gather  $\hat{\mathbf{I}}$ .

Following the same rationale of the synthetic example, we split each dataset into 250 gathers for training and validation and leave the remaining to evaluation set. Then, in order to achieve a similar number of patches per gather (i.e., 135 in the synthetic case), we extract 129 patches with size  $128 \times 128$ , overlapped on temporal dimension, specifically with patch-stride of 10 samples. Notice that, in this case, the presence of patch overlap does not cause issues in memory usage, as the number of samples entering the network is similar to the chosen configuration for the synthetic example.

Results obtained on the evaluation dataset  $\mathcal{D}_E$  are reported in Table III, while Fig. 9 shows an example of gather reconstruction where 50% of traces is missing. It is noticeable the improvement in performances of the new proposed architecture, especially for the case  $H = 50$ , where we achieve 6dB more than our previous work. This achievement is due to the specific changes performed on the *U-net* architecture as

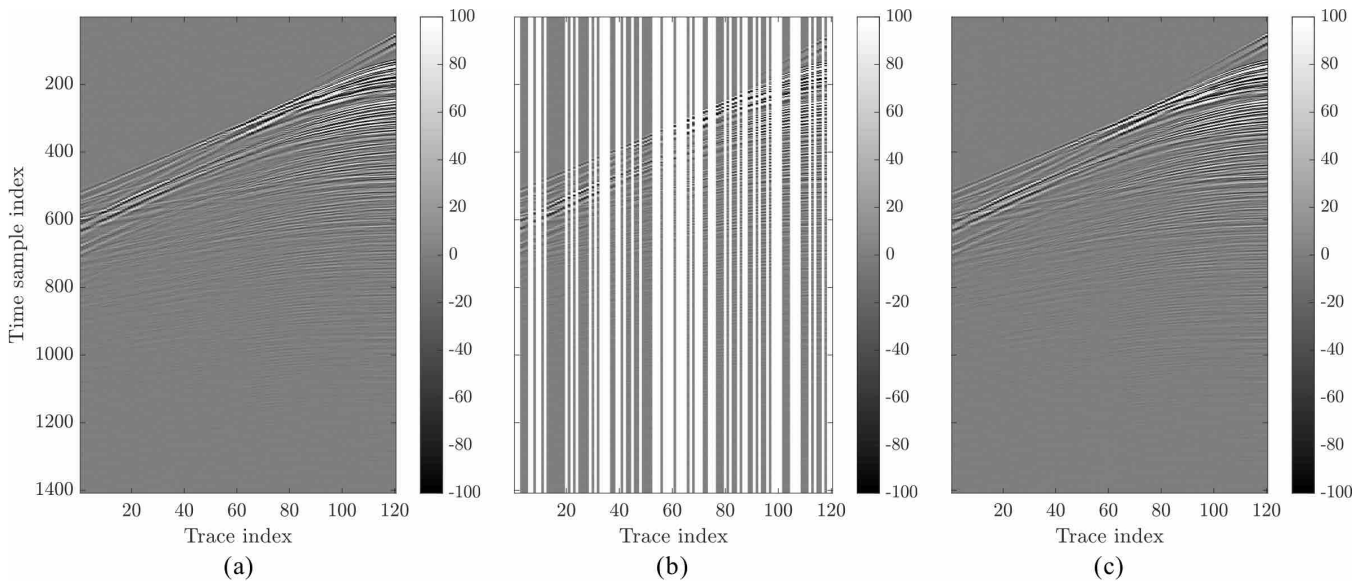


Fig. 9: Example of data interpolation, considering one gather of the field dataset [46]. Precisely, (a) depicts the original gather  $\mathbf{I}$ , (b) reports the corrupted gather  $\bar{\mathbf{I}}$ , with 50% of randomly missing traces, (c) shows the reconstructed gather  $\hat{\mathbf{I}}$ .

TABLE III: Average SNR [dB] achieved on gathers from dataset in [46].

$H$	10	30	50
New $U$ -net	25.7	20.5	16.7
Old $U$ -net	22.5	15.1	10.2

described in Section III-A. As a matter of fact, even if selecting a reduced amount of gathers for training and validation (i.e., 25% of the whole dataset instead of 75%), the resulting SNR always exceeds the past performances.

### C. Problem 2: Denoising of corrupted gathers

In this section we report the results of the experimental campaign related to denoising of corrupted gathers. We consider two kinds of additive noise, the standard Additive White Gaussian Noise (AWGN), and a spike-like noise.

Concerning the patch extraction methodology to be applied, we select exactly the same strategy of that presented in Section IV-B1a. As a matter of fact, the presence of randomly missing traces as well as the additive random noise can be seen as two generic kinds of gather corruption, which can be tackled by the  $U$ -net in a similar way.

1) *AWGN noise model*: In order to test our method over a plurality of Signal-to-Noise Ratios (SNR), we add white gaussian noise for achieving  $\text{SNR} = S \in \{-3, 0, 3\}$ dB, defined as the ratio between the image and noise variances.

The average results obtained on shot gathers belonging to the evaluation set  $\mathcal{D}_E$  are the following:  $\text{SNR} = 12.8$ dB, 14.4dB and 16.3dB, correspondent to increasing values of  $S$ . Indeed, these results can be considered an upper bound for the achievable performances of the proposed strategy in realistic scenarios. As a matter of fact, they are obtained on the assumption to have clean data available for the training phase, which is never the case for field acquired data.

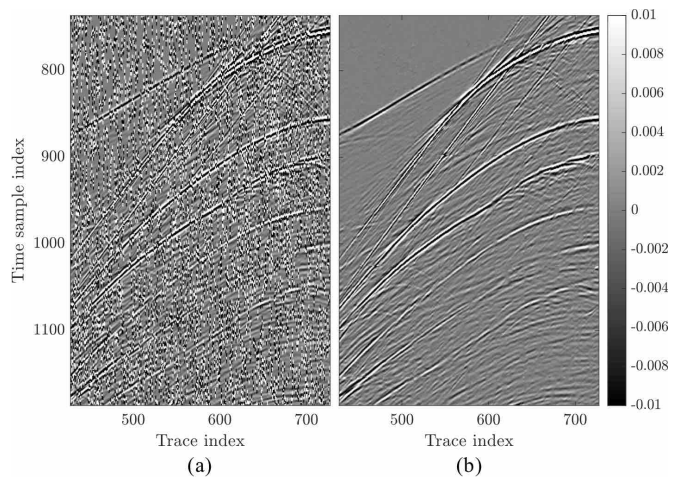


Fig. 10: Example of spike-like noise attenuation. Precisely, (a) reports the corrupted gather  $\bar{\mathbf{I}}$ , with noise density  $d = 3$ , (b) shows the reconstructed gather  $\hat{\mathbf{I}}$ .

2) *Spike-like noise model*: Pre-stack seismic data can be affected by different types of random noise coming from various sources, such as wind motion, poorly planted geophones or electrical noise, most of these being far more complex than simple AWGN. For instance, some of these seismic noises exhibit spike-like characteristics [47] and are lately gaining growing interest, as they strongly affect the processing of simultaneous source data acquired from recent seismic surveys [48].

Therefore, we propose to use our network for denoising data corrupted by additive spike-like noise. In order to simulate this noise, we add salt and pepper noise with variable density  $d\%$ , namely the percentage of corrupted samples in one gather. In particular, the binary values of this noise are set to the minimum and maximum values of the original uncorrupted



TABLE IV: Initial SNR [dB] on corrupted gathers and final SNR [dB] achieved by spike-like denoising.

$d$	1	3
Initial	-34.8	-39.6
Final	16.8	12.3

data. Then, we convolve each noise trace with a Ricker wavelet having the same central frequency of the data (i.e., 27Hz) and unit energy. This way, we generate two corrupted datasets, corresponding to  $d \in \{1, 3\}$ .

Fig. 10 shows an example of spike-like corruption denoising for  $d = 3$ . The original gather is the same of that previously shown in Fig. 6(a). It is noticeable that, even if the corrupted image visually undergoes a strong degradation, the reconstructed one presents almost all the features of the original data. This trend is confirmed by Table IV, which reports the average results achieved on set  $\mathcal{D}_E$ .

3) *Towards standard denoiser emulation*: In order to highlight the *U-net*-based method versatility, we propose to exploit our denoising strategy as an emulator of some well known standard denoising algorithms. In particular, we select two noise attenuation strategies, namely the Wavelet denoising [49] and the Wiener one [50]. To test the denoising performances, we use the datasets corrupted by AWGN with  $\text{SNR} = S \in \{-3, 0, 3\}$ dB.

Initially, we process the whole datasets through the aforementioned standard denoising algorithms. Through this operation, we are generating denoised data which can be more or less considered in the same way as clean uncorrupted gathers.

In a second phase, we train our network in a slightly different way than the approach shown in Section III-B. Indeed, we train the *U-net* substituting to ground truth gathers those obtained through denoising by Wavelet or Wiener. Thus, the training step includes pairs of noisy gathers and gathers denoised by standard algorithms. Eventually, we evaluate denoising results on shot gathers belonging to  $\mathcal{D}_E$ , comparing reconstructed gathers with the original ones, as described in (5). Specifically, we compute the average results for *U-net* and for standard denoising algorithms as well.

From results depicted in Table V it is quite evident that performances of *U-net* are comparable with those achieved through the denoising algorithm used for training, showing that *U-net* is able to mimic their performances. Moreover, the proposed method has a further advantage, which is the low computational effort in denoising a generic gather. As a matter of fact, if a risible amount of time is needed for training the network model parameters, the evaluation phase is very efficient: Wavelet-based and Wiener-based denoising, which are actually simple and efficient algorithms, take respectively the 25% and 150% more than the time required by our strategy for estimating each denoised gather.

These results pave the way towards one potential application of our method in realistic situations. Indeed, as previously stated, having clean gathers available for the training phase is not the case when dealing with real data. Furthermore, denoising field acquisitions often require complex and com-

TABLE V: Average SNR [dB] on gathers belonging to  $\mathcal{D}_E$ , training the *U-net* on gathers denoised by Wavelet (a) and Wiener (b).

$S$	-3	0	3	$S$	-3	0	3
<i>U-net</i>	4.8	5.7	6.9	<i>U-net</i>	6.6	8.1	9.9
Wavelet	4.7	5.7	6.9	Wiener	6.6	8	9.9

(a) (b)

putationally expensive algorithms.

In order to overcome these issues, we recommend our strategy as a viable alternative to many standard denoising algorithms. Specifically, when a large field dataset is available, the following pipeline can be applied:

- 1) randomly select a subset of the acquired shot gathers;
- 2) perform an accurate and computationally expensive denoising on the selected shot gathers;
- 3) train the *U-net* on the selected pairs of acquired/denoised gathers;
- 4) make use of the trained *U-net* to denoise the remaining data.

After a certain dimension of the dataset, due to the fixed computational cost for denoising the selected subset and training the *U-net*, the application of the *U-net*-based denoising becomes computationally cheaper than denoising the whole dataset with the standard noise attenuation algorithm. Indeed, the computational advantage of *U-net* increases with the dimension of the dataset and the complexity of the denoising algorithm.

#### D. Complete problem: Joint interpolation and denoising

The last situation we propose is the more realistic case of study, implying additive noise corruption jointly with missing traces. Precisely, we investigate two cases of study: the former exploits the same synthetic dataset of all the previous experiments, while the latter uses a different dataset, comparing our method with state-of-the-art techniques.

1) *AWGN and uniform missing traces*: In order to investigate if the proposed method is able to retrieve the original synthetic data, we consider the presence of AWGN and uniformly distributed missing traces. Likewise previously done, we add noise leading into  $S \in \{3, 0, -3\}$ dB and delete a percentage  $H \in \{10, 30, 50\}$  of the available data traces for simulating the lack of seismic acquisitions. This way, we generate 9 different datasets, corresponding to various combinations of additive noise and missing traces.

Table VI resumes the average results obtained on shot gathers belonging to the evaluation set  $\mathcal{D}_E$ , considering all possible combinations of missing traces and additive noise variances.

2) *Comparison with state-of-the-art*: To compare our strategy with state-of-the-art, we consider the Double-Sparsity Dictionary Learning method proposed by [29] and one strategy based on fixed dictionary transform used as baseline in [29], i.e., the Curvelet method. In order to perform a fair comparison, we reproduce exactly the same synthetic example provided in [29].

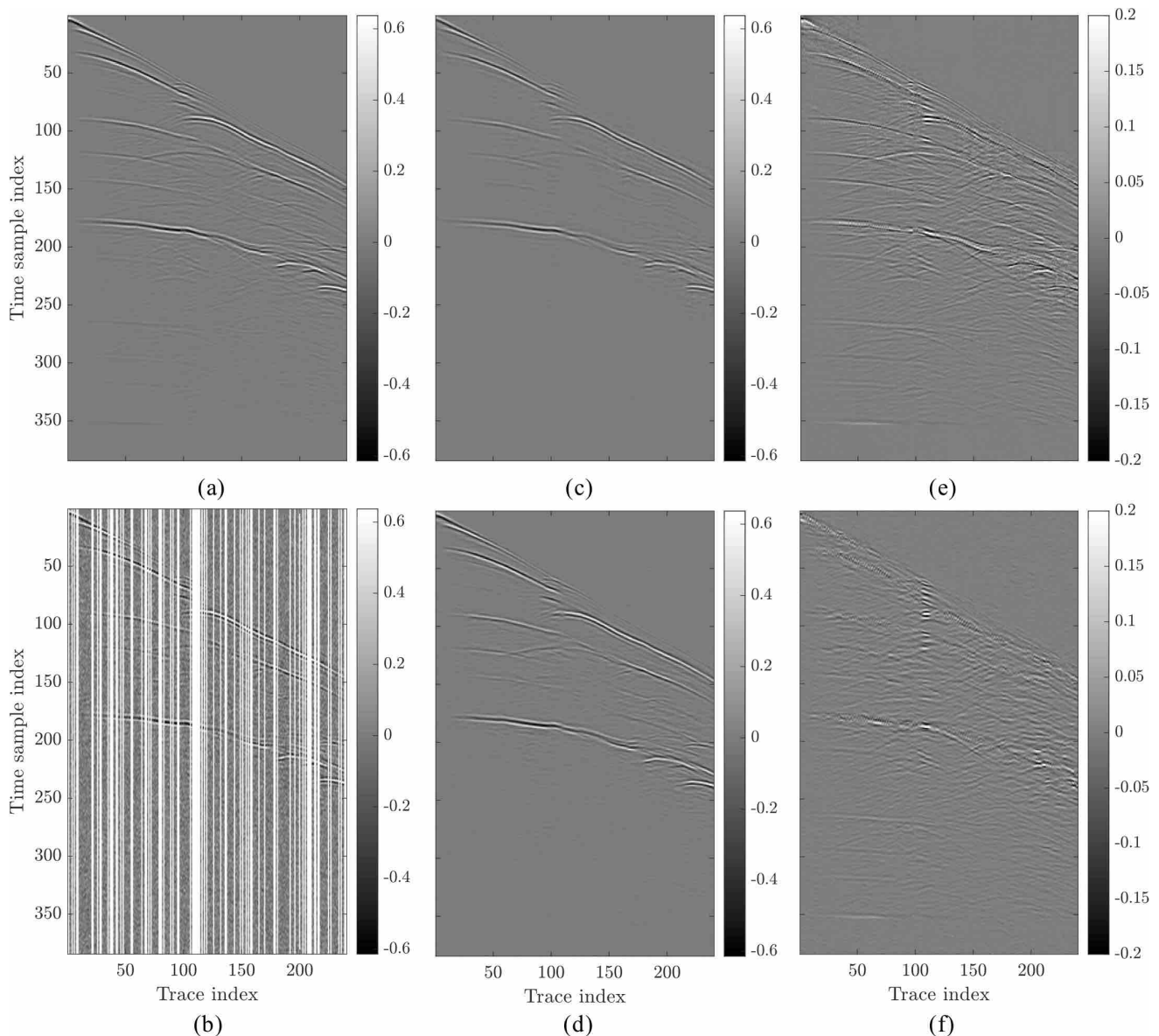


Fig. 11: Shot gather with 33% of missing traces and  $\sigma = 0.1$ . (a) shows the original gather; (b) depicts the corrupted version; (c) shows the recovered gather obtained with double-sparsity dictionary learning, PSNR = 32.1 dB; (d) shows the recovered gather obtained with *U-net*, PSNR = 33.7 dB; (e) illustrates the reconstruction error of double-sparsity dictionary learning; (f) depicts the reconstruction error of *U-net*.

TABLE VI: Average SNR [dB] achieved on gathers belonging to  $\mathcal{D}_E$ , for each dataset extracted from BP-2004 [43].

$H \backslash S$	-3	0	3
10	12.2	13.8	15.6
30	11.5	12.9	14.4
50	10.4	11.6	12.9

Specifically, the dataset is extracted from the BP-1997 benchmark [51] and includes 385 shot gathers, cropped at the last 240 receivers (taking the source as reference) with 384 samples/trace. We add noise and randomly downsample the dataset following the procedure described therein. In the first stage, as done in [29], we normalize the range of each

trace to 1. Then, white gaussian noise is generated, low pass-filtered with a cut-off frequency of 30Hz and finally added to the traces. We perform the same experimental campaign of that proposed in [29], testing plenty of noise standard deviations  $\sigma \in \{0.05, 0.10, 0.15, 0.20, 0.25\}$  and missing traces' percentages  $H \in \{10, 20, 30, 33, 40, 50, 60\}$ .

For what concerns the training phase, we randomly select 250 shot gathers for training and validation (split in 75% – 25%). In test phase, we investigate exactly the same image of that used in [29], namely the first shot gather in the dataset. Note that, in order to be fair, we never exploit this shot gather in the training phase.

During training, we extract from each image 153 overlapping patches with size  $128 \times 128$  and stride (16, 14) along rows and columns, respectively. This operation has been done

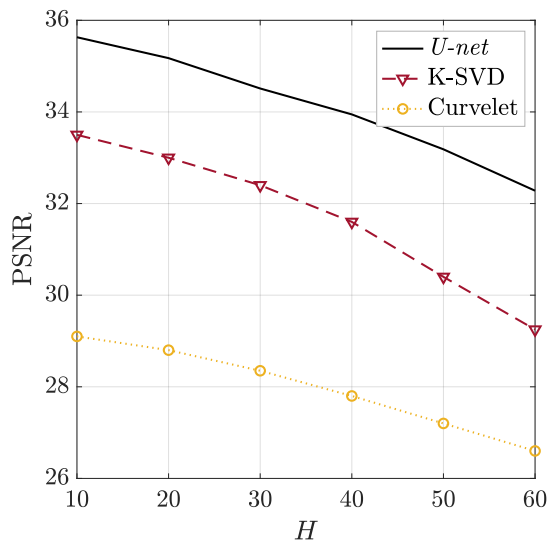


Fig. 12: Results of different reconstruction methods by varying the missing traces ratio  $H$  and for  $\sigma = 0.1$ .

in order to achieve training and validation sets with similar size (concerning the number of patches) to the previously shown situations. Notice that we consider exactly the same training-validation-evaluation pipeline of that depicted in Sections III-B and III-C.

For comparing the results, we use the evaluation metrics proposed in [29], namely the peak signal to noise ratio (PSNR), defined as

$$\text{PSNR} = 10 \log_{10} \frac{s_{\max}}{\sigma^2(\mathbf{I} - \hat{\mathbf{I}})}, \quad (7)$$

being  $s_{\max}$  the dynamic range of the clean signal, thus fixed to 1.

Fig. 11(a) shows the original shot gather without noise added and missing traces (i.e., the ground truth of the experiment). The corrupted version of the gather with 33% of missing traces and  $\sigma = 0.1$  is shown in Fig. 11(b).

Figs. 11(c)-(d) show the recovered gathers obtained with double-sparsity dictionary learning and *U-net*, respectively. Although both results are visually satisfactory, we can notice there are some events which are well reconstructed by the *U-net* while are missing in the retrieved shot gather via double-sparsity dictionary learning. Specifically, Figs. 11(e)-(f) show the error panels (i.e., the difference between the recovered images (c) and (d) and the ground truth (a)) for the results obtained with the state-of-the-art technique and *U-net* respectively. Please note that the axis scale of error panels is changed with respect to that related to gathers, in order to enhance the details. It is quite evident that the error corresponding to double-sparsity dictionary learning is more affected by residual coherent events, meaning that those are not correctly recovered. These qualitative considerations are confirmed by the corresponding PSNR values: 32.1 dB for double-sparsity dictionary learning and 33.7 dB for *U-net*.

Fig. 12 displays the performances of different reconstruction methods by varying the missing traces ratio and selecting  $\sigma = 0.1$ . In particular, we compare results reported in [29] with our results, averaged over 100 different realizations of

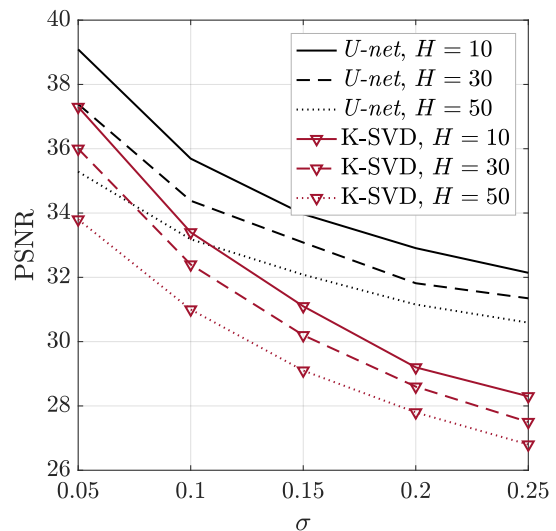


Fig. 13:  $H = \{10, 30, 50\}$ ,  $\sigma = 0.05 : 0.05 : 0.25$

the column pattern used for randomly deleting the traces. It is noticeable that we significantly outperform both the dictionary learning-based method and the Curvelet-based, gaining an average of 2.4 dB with respect to the former strategy and 6.1 dB to the latter one.

Fig. 13 reports the achieved results for a plurality of noise standard deviations. The performances of the *U-net* are significantly superior than those of dictionary learning-based strategy, in all the examined cases. Moreover, our method reveals to be more robust in presence of strong noise. As a matter of fact, as noise standard deviation  $\sigma$  increases, the curves related to state-of-the-art method decay in a worse fashion than ours, to the point that we can achieve PSNR = 30.3 dB for  $H = 50$  and  $\sigma = 0.25$ , against the 26.7 dB of the dictionary learning-based technique.

## V. CONCLUSIONS

In this paper, we proposed a method for reconstruction of corrupted seismic data, focusing on noise attenuation and interpolation of missing pre-stack data traces in the shot-gather domain. In particular, we considered random noises with different statistics and a plurality of missing traces distribution. Our approach makes use of a convolutional neural network architecture for interpolation and denoising of 2D shot gathers, showing significant performance improvements with respect to state-of-the-art solutions for joint denoising and interpolation.

Results achieved on controlled synthetic experiments demonstrate that the proposed method is a promising strategy for seismic data pre-processing. Moreover, once the network training procedure is completed, processing data with our strategy is also quite efficient in terms of computational effort.

We examined also the potential application of our methodology on field data for production environments. In this situation, it is interesting to notice that the proposed algorithm can be used also to emulate the effect of more time consuming classical data pre-processing strategies.

Future work will be devoted to investigate issues related to denoising of field data, exploring for instance the feasibility of

a transfer learning procedure by training convolutional neural networks on properly designed synthetic data and testing on field data. Moreover, investigations are needed for denoising of more challenging types of coherent noise and artifacts affecting seismic data (e.g., ground roll in land data).

Further studies on the network architectures and loss functions could relax the need of corrupted/uncorrupted pairs of gathers for the training set, thus helping in dealing with the problem of building a training dataset for denoising.

Finally, another aspect we would like to examine for moving towards production environments is the extension of the proposed procedure to 3D data.

In the light of the promising results achieved with the proposed architecture of convolutional neural network, we believe this tool can pave the way towards even more efficient and accurate solutions.

## REFERENCES

- [1] W. F. Chang and G. A. McMechan, "3d acoustic prestack reverse-time migration," *Geophysical Prospecting*, vol. 38, no. 7, pp. 737–755, 1990.
- [2] J. Virieux and S. Operto, "An overview of full-waveform inversion in exploration geophysics," *Geophysics*, vol. 74, no. 6, pp. WCC1–WCC26, 2009.
- [3] D. J. Verschuur, A. J. Berkhout, and C. P. A. Wapenaar, "Adaptive surface related multiple elimination," *Geophysics*, vol. 57, no. 9, pp. 1166–1177, 1992.
- [4] R. H. Stolt, "Seismic data mapping and reconstruction," *Geophysics*, vol. 67, no. 3, pp. 890–908, 2002.
- [5] S. Fomel, "Seismic reflection data interpolation with differential offset and shot continuation," *Geophysics*, vol. 68, no. 2, pp. 733–744, 2003.
- [6] S. Spitz, "Seismic trace interpolation in the fx domain," *Geophysics*, vol. 56, no. 6, pp. 785–794, 1991.
- [7] S. R. Trickett, "F-xy eigenimage noise suppression," *Geophysics*, vol. 68, no. 2, pp. 751–759, 2003.
- [8] S. Trickett and L. Burroughs, "Prestack rank-reducing noise suppression: Theory," in *SEG Technical Program Expanded Abstracts 2009*. Society of Exploration Geophysicists, 2009, pp. 3332–3336.
- [9] V. Oropeza and M. Sacchi, "Simultaneous seismic data denoising and reconstruction via multichannel singular spectrum analysis," *Geophysics*, vol. 76, no. 3, pp. V25–V32, 2011.
- [10] Y. Yang, J. Ma, and S. Osher, "Seismic data reconstruction via matrix completion," *Inverse Problems and Imaging*, vol. 7, no. 4, pp. 1379–1392, 2013.
- [11] R. Kumar, A. Y. Aravkin, E. Esser, H. Mansour, and F. J. Herrmann, "Svd-free low-rank matrix factorization-wavefield reconstruction via jittered subsampling and reciprocity," in *76th EAGE Conference and Exhibition 2014*, 2014.
- [12] A. Adamo, P. Mazzucchelli, and N. Bienati, "Irregular interpolation of seismic data through low-rank tensor approximation," in *Geoscience and Remote Sensing Symposium (IGARSS), 2015 IEEE International*. IEEE, 2015, pp. 4292–4295.
- [13] M. Naghizadeh, "Seismic data interpolation and denoising in the frequency-wavenumber domain," *Geophysics*, vol. 77, no. 2, pp. V71–V80, 2012.
- [14] B. M. Battista, C. Knapp, T. McGee, and V. Goebel, "Application of the empirical mode decomposition and hilbert-huang transform to seismic reflection data," *Geophysics*, vol. 72, no. 2, pp. H29–H37, 2007.
- [15] M. Bekara and M. Van der Baan, "Random and coherent noise attenuation by empirical mode decomposition," *Geophysics*, vol. 74, no. 5, pp. V89–V98, 2009.
- [16] N. Wu, Y. Li, and B. Yang, "Noise attenuation for 2-d seismic data by radial-trace time-frequency peak filtering," *IEEE Geoscience and Remote Sensing Letters*, vol. 8, no. 5, pp. 874–878, 2011.
- [17] Y. Liu, Y. Li, P. Nie, and Q. Zeng, "Spatiotemporal time–frequency peak filtering method for seismic random noise reduction," *IEEE Geoscience and Remote Sensing Letters*, vol. 10, no. 4, pp. 756–760, 2013.
- [18] Y. Tian and Y. Li, "Parabolic-trace time-frequency peak filtering for seismic random noise attenuation," *IEEE Geoscience and Remote Sensing Letters*, vol. 11, no. 1, pp. 158–162, 2014.
- [19] J. Wang, M. Ng, and M. Perz, "Seismic data interpolation by greedy local radon transform," *Geophysics*, vol. 75, no. 6, pp. WB225–WB234, 2010.
- [20] F. J. Herrmann and G. Hennenfent, "Non-parametric seismic data recovery with curvelet frames," *Geophysical Journal International*, vol. 173, no. 1, pp. 233–248, 2008.
- [21] S. Gan, S. Wang, Y. Chen, Y. Zhang, and Z. Jin, "Dealiased seismic data interpolation using seislet transform with low-frequency constraint," *IEEE Geoscience and remote sensing letters*, vol. 12, no. 10, pp. 2150–2154, 2015.
- [22] B. Wang, R.-S. Wu, Y. Geng, and X. Chen, "Dreamlet-based interpolation using pocs method," *Journal of Applied Geophysics*, vol. 109, pp. 256–265, 2014.
- [23] R. Zhang and T. J. Ulrych, "Physical wavelet frame denoising," *Geophysics*, vol. 68, no. 1, pp. 225–231, 2003.
- [24] F. J. Herrmann, P. Moghaddam, and C. C. Stolk, "Sparsity-and continuity-promoting seismic image recovery with curvelet frames," *Applied and Computational Harmonic Analysis*, vol. 24, no. 2, pp. 150–173, 2008.
- [25] S. Fomel and Y. Liu, "Seislet transform and seislet frame," *Geophysics*, vol. 75, no. 3, pp. V25–V38, 2010.
- [26] Y. Chen\* and S. Fomel, "Emd-seislet transform," in *SEG Technical Program Expanded Abstracts 2015*. Society of Exploration Geophysicists, 2015, pp. 4775–4778.
- [27] L. Zhu, E. Liu, and J. H. McClellan, "Seismic data denoising through multiscale and sparsity-promoting dictionary learning," *Geophysics*, vol. 80, no. 6, pp. WD45–WD57, 2015.
- [28] Y. Chen, J. Ma, and S. Fomel, "Double-sparsity dictionary for seismic noise attenuation," *Geophysics*, vol. 81, no. 2, pp. V103–V116, 2016.
- [29] L. Zhu, E. Liu, and J. H. McClellan, "Joint seismic data denoising and interpolation with double-sparsity dictionary learning," *Journal of Geophysics and Engineering*, vol. 14, no. 4, p. 802, 2017.
- [30] B. Wang, N. Zhang, W. Lu, P. Zhang, and J. Geng, "Seismic data interpolation using deep learning based residual networks," in *80th EAGE Conference and Exhibition 2018*, 2018.
- [31] Y. Jin, X. Wu, J. Chen, Z. Han, and W. Hu, "Seismic data denoising by deep-residual networks," in *SEG Technical Program Expanded Abstracts 2018*. Society of Exploration Geophysicists, 2018, pp. 4593–4597.
- [32] A. Siahkoobi, R. Kumar, and F. Herrmann, "Seismic data reconstruction with generative adversarial networks," in *80th EAGE Conference and Exhibition 2018*, 2018.
- [33] S. Mandelli, F. Borra, V. Lipari, P. Bestagini, A. Sarti, and S. Tubaro, "Seismic data interpolation through convolutional autoencoder," in *SEG Technical Program Expanded Abstracts 2018*. Society of Exploration Geophysicists, 2018, pp. 4101–4105.
- [34] A. Mikhailliuk and A. Faul, "Deep learning applied to seismic data interpolation," in *80th EAGE Conference and Exhibition 2018*, 2018.
- [35] O. Ronneberger, P. Fischer, and T. Brox, "U-net: Convolutional networks for biomedical image segmentation," in *International Conference on Medical image computing and computer-assisted intervention*. Springer, 2015, pp. 234–241.
- [36] J. Xie, L. Xu, and E. Chen, "Image denoising and inpainting with deep neural networks," in *Proceedings of the 25th International Conference on Neural Information Processing Systems - Volume 1*, ser. NIPS'12. USA: Curran Associates Inc., 2012, pp. 341–349.
- [37] D. Pathak, P. Krahenbuhl, J. Donahue, T. Darrell, and A. A. Efros, "Context encoders: Feature learning by inpainting," in *Proceedings of the IEEE Conference on Computer Vision and Pattern Recognition*, 2016, pp. 2536–2544.
- [38] K. H. Jin, M. T. McCann, E. Froustey, and M. Unser, "Deep convolutional neural network for inverse problems in imaging," *IEEE Transactions on Image Processing*, vol. 26, no. 9, pp. 4509–4522, 2017.
- [39] Z. Yan, X. Li, M. Li, W. Zuo, and S. Shan, "Shift-net: Image inpainting via deep feature rearrangement," in *Computer Vision - ECCV 2018 - 15th European Conference, Munich, Germany, September 8-14, 2018, Proceedings, Part XIV*, 2018, pp. 3–19. [Online]. Available: [https://doi.org/10.1007/978-3-030-01264-9\\_1](https://doi.org/10.1007/978-3-030-01264-9_1)
- [40] G. Liu, F. A. Reda, K. J. Shih, T. Wang, A. Tao, and B. Catanzaro, "Image inpainting for irregular holes using partial convolutions," in *Computer Vision - ECCV 2018 - 15th European Conference, Munich, Germany, September 8-14, 2018, Proceedings, Part XI*, 2018, pp. 89–105. [Online]. Available: [https://doi.org/10.1007/978-3-030-01252-6\\_6](https://doi.org/10.1007/978-3-030-01252-6_6)
- [41] M. P. Heinrich, M. Stille, and T. M. Buzug, "Residual u-net convolutional neural network architecture for low-dose ct denoising," *Current Directions in Biomedical Engineering*, vol. 4, no. 1, pp. 297–300, 2018.
- [42] D. P. Kingma and J. Ba, "Adam: A method for stochastic optimization," *arXiv preprint arXiv:1412.6980*, 2014.

- [43] F. Billette and S. Brandsberg-Dahl, "The 2004 bp velocity benchmark," in *67th EAGE Conference & Exhibition*, 2005.
- [44] Y. Chen, L. Zhang, and L.-w. Mo, "Seismic data interpolation using non-linear shaping regularization," *Journal of Seismic Exploration*, vol. 24, pp. 327–342, 2015.
- [45] B. P. Milner and A. B. James, "An analysis of packet loss models for distributed speech recognition," in *Eighth International Conference on Spoken Language Processing*, 2004.
- [46] R. G. Keys and D. J. Foster, "A data set for evaluating and comparing seismic inversion methods," *Comparison of seismic inversion methods on a single real data set*, pp. 1–12, 1998.
- [47] Y. Liu, C. Liu, and D. Wang, "A 1d time-varying median filter for seismic random, spike-like noise elimination," *Geophysics*, vol. 74, no. 1, pp. V17–V24, 2008.
- [48] Y. Zhou, C. Shi, H. Chen, J. Xie, G. Wu, and Y. Chen, "Spike-like blending noise attenuation using structural low-rank decomposition," *IEEE Geoscience and Remote Sensing Letters*, vol. 14, no. 9, pp. 1633–1637, 2017.
- [49] E. Jones, T. Oliphant, and P. Peterson, "Scipy: Open source scientific tools for python," 2001.
- [50] S. Van der Walt, J. L. Schönberger, J. Nunez-Iglesias, F. Boulogne, J. D. Warner, N. Yager, E. Gouillart, and T. Yu, "scikit-image: image processing in python," *PeerJ*, vol. 2, p. e453, 2014.
- [51] J. Etgen and C. Regone, "Strike shooting, dip shooting, widepatch shooting does prestack depth migration care? a model study," in *SEG Technical Program Expanded Abstracts 1998*. Society of Exploration Geophysicists, 1998, pp. 66–69.